

# Electron transport through nuclear pasta in magnetized neutron stars

D. G. Yakovlev<sup>\*</sup>

*Ioffe Physical Technical Institute, 26 Politekhnicheskaya, St. Petersburg 194021, Russia*

Accepted . Received ; in original form

## ABSTRACT

We present a simple model for electron transport in a possible layer of exotic nuclear clusters (in the so called nuclear pasta layer) between the crust and liquid core of a strongly magnetized neutron star. The electron transport there can be strongly anisotropic and gyrotropic. The anisotropy is produced by different electron effective collision frequencies along and across local symmetry axis in domains of exotic ordered nuclear clusters and by complicated effects of the magnetic field. We also calculate averaged kinetic coefficients in case local domains are freely oriented. Possible applications of the obtained results and open problems are outlined.

**Key words:** dense matter – conduction – stars: neutron

## 1 INTRODUCTION

Neutron stars are thought to consist of the outer crust, inner crust and the core (e.g., Shapiro & Teukolsky 1983; Haensel, Potekhin & Yakovlev 2007). The outer crust extends to densities  $\rho \leq \rho_{\text{ND}}$ , where  $\rho_{\text{ND}} \sim (4 - 6) \times 10^{11} \text{ g cm}^{-3}$  is the neutron drip density. It mostly contains strongly degenerate electrons and atomic nuclei (remnants of atoms fully ionized by the huge electron pressure). When the density increases, the nuclei become more neutron rich.

The inner crust (where  $\rho_{\text{ND}} \leq \rho \leq \rho_{\text{cc}}$ ,  $\rho_{\text{cc}} \approx \rho_0/2$  being the density at the crust-core interface and  $\rho_0 \approx 2.8 \times 10^{14} \text{ g cm}^{-3}$  is the density of saturated nuclear matter) consists of ultrarelativistic highly degenerate electrons, very neutron rich nuclei and free degenerate neutrons (dripped off the nuclei). With increasing density in the inner crust, the fraction of free neutrons (among bound and free nucleons) grows up, so that free neutrons give larger contribution to the pressure, while atomic nuclei become loosely bound as if dissolving in the neutron sea. Finally, the nuclei disappear at  $\rho_{\text{cc}}$  which signals the transition to the liquid core of the star. The crust as a whole is about 1 km thick and contains about one percent of the neutron star mass.

The liquid core can extend to about  $10\rho_0$ . The outer core ( $\rho_{\text{cc}} \leq \rho \leq 2\rho_0$ ) consists of strongly degenerate neutrons, with some admixture of protons, electrons and muons. The inner core ( $\rho \geq 2\rho_0$ ) may contain hyperons, pion or kaon condensates or free quarks or the mixture of these.

The aim of this paper is to study a possible layer of *nuclear mantle* at the bottom of the inner crust containing various *exotic nuclear clusters* called collectively *nuclear pasta*. It was predicted by Ravenhall, Pethick & Wilson (1983) who investigated properties of matter in core-collapsing supernovae. It has been studied by many authors as summarized in a discussion below (also see Haensel,

Potekhin & Yakovlev 2007 for references to early publications). A neutron star mantle can exist or not, depending on specific properties of nuclear interactions at subnuclear densities. If exist, it forms the layer between the ordinary crust and the core,  $\rho_{\text{cm}} \leq \rho \leq \rho_{\text{cc}}$ , where  $\rho_{\text{cm}} \approx 10^{14} \text{ g cm}^{-3}$  is the outer boundary of this layer. The mantle is often viewed as a part of the inner crust. Although the mantle occurs in a narrow density interval, its mass can be comparable to the mass of the entire crust. As remarked above, the nuclei are loosely bound there. In this case nuclear binding becomes as low as Coulomb energies of the nuclei. Nuclear pasta forms when Coulomb energy is sufficiently strong to rearrange nearly spherical atomic nuclei into exotic nuclear clusters.

The studies of nuclear pasta can be divided into two parts. First, one considers hot matter of subnuclear densities for core-collapsed supernovae and proto-neutron stars where beta equilibrium is absent. The second direction is to investigate colder pasta that can be available in neutron stars under the beta equilibrium condition. We are interested in the second possibility. Very roughly, a transition from the first to the second case occurs at temperatures  $T$  from about a few times of  $10^9 \text{ K}$  to  $\sim 10^{10} \text{ K}$ .

There are two major approaches to study nuclear pasta.

(i) First, one considers one-, two- or three dimensional nuclear clusters using different versions of the compressible liquid drop model (e.g., Ravenhall, Pethick & Wilson 1983; Hashimoto, Seki & Yamada 1984; Lorenz, Ravenhall & Pethick 1993; Watanabe, Iida & Sato 2000; Watanabe & Iida 2003; Nakazato, Oyamatsu & Yamada 2009) or Thomas-Fermi theories (e.g., Williams & Koonin 1985; Oyamatsu 1993; Okamoto et al. 2013; Grill et al. 2014) with various mean field interactions. The theory predicts four phases I–IV of nuclear pasta in a neutron star mantle. The first phase I, which appears with increasing density at  $\rho > \rho_{\text{cm}}$ , is the phase of rods (“spaghetti”). Nuclear structures become rod-like there, immersed in a liquid of free neutrons. One studies neutron and proton density profiles across these rods assuming that their length is large (infi-

<sup>\*</sup> E-mail: yak.astro@mail.ioffe.ru

nite). The phase of rods is followed by phase II of slabs (“lasagna” phase). The slabs are filled by nuclear matter and immersed in neutron liquid. One calculates nuclear structure across the slabs while the slabs themselves are assumed large (infinite). The phase of slabs is followed by phase III of rod-like bubbles (“anti-spaghetti”), where free neutrons fill infinitely long bubbles aligned along certain axis, and the nuclear structures occupy all other space. The final phase IV consists of nuclear matter with spherical bubbles of neutron (and possibly proton) liquid (“Swiss cheese”). Some calculations predict all four exotic phases, while others predict fewer phases or no exotic phases at all. Real rods or slabs are thought to be of finite size and occupy some domains. The sizes of nuclear clusters and domains as well as orientations of nuclear clusters in different domains are uncertain.

(ii) Second, one simulates the composition and dynamics of ensembles of nuclear clusters with various versions of quantum molecular dynamics (e.g., Maruyama et al. 1998; Kido et al. 2000; Watanabe et al. 2002; Schuetrumpf et al. 2015) or classical molecular dynamics (e.g., Horowitz et al. 2004, 2005; Dorso, Giménez Molinelli & López 2012; Caplan et al. 2014; Horowitz et al. 2015). Such simulations predict a variety of possibilities, first of all nuclear clusters of one type, e.g. rods, but of finite lengths and different sizes. They predict also mixtures of different clusters (e.g., rods and slabs). Recently, more exotic structures have been obtained, such as slabs with a lattice of bubbles (“nuclear waffles,” Schneider et al. 2014), gyroids (Nakazato, Oyamatsu & Yamada 2009; Schuetrumpf et al. 2015), intertwined lasagna and other structures which do not resemble usual pasta (Alcain, Giménez Molinelli & Dorso 2014), as well as long lived topological defects (e.g., Horowitz et al. 2015). At high temperatures  $T \gtrsim 10^{10}$  K nuclear pasta is mostly in liquid state but at low temperatures (in neutron stars) it freezes into ordered or disordered clusters.

The existence of nuclear pasta does not affect significantly the equation of state of the matter and neutron star models. However it can strongly influence neutrino emission (e.g., Lorenz, Ravenhall & Pethick 1993; Kaminker et al. 1999; Gusakov et al. 2004; Horowitz et al. 2005) and transport properties of the neutron star mantle (e.g., Pons, Viganò & Rea 2013; Horowitz et al. 2015). We will focus on electron transport which is thought to be dominant there. To simplify the problem we assume the existence of nuclear pasta domains with nuclear clusters of one type in each domain. We include the effects of strong magnetic fields which can be very important.

## 2 ONE DOMAIN

### 2.1 General expressions

We start with the electron transport properties in one domain assuming that electron mean free paths are larger than spacing between nuclear clusters but smaller than domain size and neglecting boundary effects. For example, consider ensembles of rod-like or slab-like nuclear structures. The electrons are mainly scattered by proton charge distributions created by these structures.

Consider a strongly degenerate and ultra-relativistic electron gas which is slightly out of thermodynamic equilibrium due to the presence of weak gradients of temperature  $T$  and electron chemical potential  $\mu$  as well as due to a weak electric field  $\mathbf{E}$ . Kinetic properties of the electrons are calculated from the Boltzmann equation

for the electron distribution function  $f(\mathbf{r}, \mathbf{p}, t)$ ,

$$\frac{df}{dt} \equiv \frac{\partial f}{\partial t} + \mathbf{v} \cdot \frac{\partial f}{\partial \mathbf{r}} - e \left( \mathbf{E} + \frac{\mathbf{v}}{c} \times \mathbf{B} \right) \cdot \frac{\partial f}{\partial \mathbf{p}} = I\{f\}, \quad (1)$$

where  $\mathbf{v}$ ,  $\mathbf{p}$  and  $-e$  are the electron velocity, momentum and electric charge, respectively;  $\mathbf{B}$  is the external magnetic field, and  $I\{f\}$  is the collision integral. The distribution function is normalized as

$$n_e(\mathbf{r}, t) = \frac{2}{(2\pi\hbar)^3} \int d^3\mathbf{p} f(\mathbf{r}, \mathbf{p}, t), \quad (2)$$

$n_e$  being the electron number density. Without any loss of generality it is sufficient to consider a stationary problem, with  $\partial f/\partial t = 0$ . Because the electrons deviate from equilibrium only slightly, we can set  $f = f_0 + \delta f$ , where

$$f_0 = \left[ \exp \left( \frac{\epsilon - \mu}{k_B T} \right) + 1 \right]^{-1} \quad (3)$$

is the local equilibrium Fermi distribution ( $\epsilon$  being the electron energy and  $k_B$  the Boltzmann constant), and  $\delta f$  is a small non-equilibrium correction.

It is well known (e.g., Pitaevskii & Lifshits 1981) that one can set  $f = f_0$  on the left-hand side of (1) in all the terms except for the one containing the magnetic force (because the latter term vanishes at  $f = f_0$ ). Then

$$\mathbf{v} \cdot \frac{\partial f_0}{\partial \mathbf{r}} - e \mathbf{E} \cdot \frac{\partial f_0}{\partial \mathbf{p}} - e \left( \frac{\mathbf{v}}{c} \times \mathbf{B} \right) \cdot \frac{\partial \delta f}{\partial \mathbf{p}} = I\{\delta f\}, \quad (4)$$

where  $I\{\delta f\}$  is the linearized collision integral.

Since  $f_0$  depends on  $\mathbf{r}$  through  $T(\mathbf{r})$  and  $\mu(\mathbf{r})$ , equation (4) can be rewritten as

$$\mathbf{v} \cdot \mathbf{F} - e \left( \frac{\mathbf{v}}{c} \times \mathbf{B} \right) \cdot \frac{\partial \delta f}{\partial \mathbf{p}} = I\{\delta f\}, \quad (5)$$

where we have introduced the notations

$$\mathbf{F} = \left( -\frac{\partial f_0}{\partial \epsilon} \right) \left( e \mathbf{E}_* + \frac{\epsilon - \mu}{T} \nabla T \right), \quad \mathbf{E}_* = \mathbf{E} + \frac{\nabla \mu}{e}, \quad (6)$$

$\mathbf{E}_*$  being the effective electric field. While calculating the electron kinetic coefficients we can treat  $\nabla T$ ,  $\nabla \mu$ ,  $\mathbf{E}$  and  $\mathbf{E}_*$  as arbitrary constant small vectors.

At the next step we should specify the linearized collision integral  $I\{\delta f\}$ . In order to study the main properties of kinetic coefficients one can often use the traditional simplified relaxation time approximation,

$$I\{\delta f\} = -\frac{\delta f}{\tau} = -\nu \delta f, \quad (7)$$

where  $\tau$  is the relaxation time and  $\nu = 1/\tau$  is the effective collision frequency. In the simplest case when electrons scatter elastically by some heavy centers, one has  $\nu = n_i \nu \sigma_{tr}$ , where  $n_i$  is the number density of scatterers and  $\sigma_{tr}$  is the transport cross section;  $\nu$ ,  $\tau$  and  $\sigma_{tr}$  can depend on the electron energy  $\epsilon$ . If one interests in a dipole-like deviation of the electron distribution function from the equilibrium one (which is relevant for studying electric and thermal conductivities as well as thermopower), it is sufficient to set  $\delta f = \mathbf{v} \cdot \mathbf{u}$ , where the vector  $\mathbf{u}$  (to be determined) can depend on the electron energy  $\epsilon$  but not on orientation of its momentum  $\mathbf{p}$ . Then  $I\{\delta f\} = -\nu \mathbf{v} \cdot \mathbf{u}$ .

The case of nuclear pasta is more complicated because we deal with anisotropic medium. As far as nuclear clusters are concerned, we assume that we have a symmetry plane ( $x, y$ ) (perpendicular to nuclear rods or plates) and a symmetry axis  $z$  (perpendicular to the plane). Without any loss of generality we may assume that the magnetic field  $\mathbf{B}$  lies in the ( $x, z$ ) plane.

**Table 1.** Possible pasta phases in a neutron star mantle

| Number | Phase             | Leading $\nu$   | Weaker $\nu$ |
|--------|-------------------|-----------------|--------------|
| I      | Rods              | $\nu_p$         | $\nu_a$      |
| II     | Slabs             | $\nu_a$         | $\nu_p$      |
| III    | Rod-like bubbles  | $\nu_p$         | $\nu_a$      |
| IV     | Spherical bubbles | $\nu_a = \nu_p$ | —            |

A natural generalization of the relaxation time approximation (7) to this case is

$$I\{\delta f\} = -\nu_a \nu_z u_z - \nu_p \mathbf{v}_p \cdot \mathbf{u}_p, \quad (8)$$

where  $\nu_a$  and  $\nu_p$  are generally different effective collision frequencies along the symmetry axis and in the symmetry plane, respectively;  $\mathbf{v}_p = (v_x, v_y)$ ;  $\mathbf{u}_p = (u_x, u_y)$ , and  $\mathbf{u}$ , as before, can depend on  $\epsilon$  but not on orientation of  $\mathbf{p}$ . The difference between  $\nu_a$  and  $\nu_p$  reflects the anisotropy of electron collision frequencies in non-spherical nuclear clusters. Such an approximation is often used for studying electron transport in anisotropic solids (see, e.g., Askerov 1981). In the absence of anisotropy, one has  $\nu_a = \nu_p$  and the problem reduces to a single traditional effective scattering frequency (7) in isotropic medium.

As discussed in Section 1, there could be four phases I–IV of nuclear pasta in a neutron star mantle; they are listed in Table 1 in order of appearance with increasing density at  $\rho > \rho_{\text{cm}}$ . Phase I consists of rods. Form symmetry consideration one can expect that the most frequent electron momentum transfer occurs when electrons move across the symmetry axis (across the rods), so that  $\nu_p$  should be larger than  $\nu_a$ . We will call  $\nu_p$  the leading collision frequency and  $\nu_a$  the weaker collision frequency (in phase I).

Phase I is followed by phase II of slabs (Table 1). Now the leading collision frequency  $\nu_a$  corresponds to electrons moving along the symmetry axis; they can scatter effectively by slabs which are perpendicular to the axis. The weaker collision frequency is then  $\nu_p$ .

After slabs one has phase III of rod-like bubbles, where the collision frequencies are expected to have the same ordering as in phase I,  $\nu_p \gg \nu_a$ .

The final phase IV is that of spherical bubbles. In this case  $\nu_a = \nu_p$  (electron collisions are isotropic) as in the case of ordinary spherical nuclei in the main body of the neutron star crust (at  $\rho < \rho_{\text{cm}}$ ).

For example, according to model I of Oyamatsu (1993),  $\rho_{\text{mc}} = 0.973 \times 10^{14} \text{ g cm}^{-3}$ . The transition to phase II occurs at  $\rho = 1.24 \times 10^{14} \text{ g cm}^{-3}$ ; to phase III at  $\rho = 1.37 \times 10^{14} \text{ g cm}^{-3}$ , and to phase IV at  $\rho = 1.42 \times 10^{14} \text{ g cm}^{-3}$ . Finally, phase IV ends at  $\rho_{\text{cc}} = 1.43 \times 10^{14} \text{ g cm}^{-3}$ . In a typical neutron star of mass  $1.4 M_\odot$  and radius about 12 km the nuclear pasta layer can be about 100 m thick and have mass  $\sim 0.01 M_\odot$ ; it is nearly as massive as the entire overlying ordinary crust of spherical nuclei.

Equation (8) reduces the linearized Boltzmann equation (5) to

$$\mathbf{v} \cdot \mathbf{F} - \omega (\mathbf{v} \times \mathbf{b}) \cdot \mathbf{u} = -\nu_a \nu_z u_z - \nu_p \mathbf{v}_p \cdot \mathbf{u}_p, \quad (9)$$

where  $\omega = eBc/\epsilon$  is the electron gyrofrequency ( $\epsilon$  includes the electron rest-mass energy), and  $\mathbf{b} = \mathbf{B}/B$  is the unit vector in the direction of  $\mathbf{B}$ . In the matrix form

$$\begin{pmatrix} -\nu_p & -\omega b_z & 0 \\ \omega b_z & -\nu_p & -\omega b_x \\ 0 & \omega b_x & -\nu_a \end{pmatrix} \begin{pmatrix} u_x \\ u_y \\ u_z \end{pmatrix} = \begin{pmatrix} F_x \\ F_y \\ F_z \end{pmatrix}. \quad (10)$$

The solution can be written as

$$u_\alpha = -\frac{1}{\Delta} A_{\alpha\beta} F_\beta, \quad (11)$$

where  $\Delta = \nu_p^2 \nu_a + \omega^2 (\nu_p b_x^2 + \nu_a b_z^2)$ . The matrix  $A_{\alpha\beta}$ , which will be denoted as  $\hat{A}$ , is

$$\hat{A} = \begin{pmatrix} \nu_a \nu_p + \omega^2 b_x^2 & -\omega b_z \nu_a & \omega^2 b_x b_z \\ \omega b_z \nu_a & \nu_a \nu_p & -\omega b_x \nu_p \\ \omega^2 b_x b_z & \omega b_x \nu_p & \nu_p^2 + \omega^2 b_z^2 \end{pmatrix}, \quad (12)$$

where  $b_z = \cos \theta$ ,  $b_x = \sin \theta$  and  $\theta$  is the angle between  $\mathbf{B}$  and the symmetry axis  $z$ .

This gives us the vector  $\mathbf{u}$  and  $f = f_0 + \delta f$ . Then we can calculate the densities of electric and thermal currents,

$$\mathbf{j} = -\frac{2e}{(2\pi\hbar)^3} \int d^3p \mathbf{v} f, \quad \mathbf{q} = \frac{2}{(2\pi\hbar)^3} \int d^3p \mathbf{v} (\epsilon - \mu) f. \quad (13)$$

Formally,  $\mathbf{j}$  and  $\mathbf{q}$  have the following structure

$$\mathbf{j} = \hat{\sigma} \mathbf{E}_* + \hat{\beta} \nabla T, \quad \mathbf{q} = -\hat{\beta} T \mathbf{E}_* - \hat{\eta} \nabla T, \quad (14)$$

where hat means  $3 \times 3$  matrix (tensor) of anisotropic kinetic coefficients,  $\hat{\sigma}$  is the electric conductivity tensor, while two other tensors,  $\hat{\beta}$  and  $\hat{\eta}$ , are auxiliary. The same tensor  $\hat{\beta}$  enters both expressions, for  $\mathbf{j}$  and  $\mathbf{q}$ , as a consequence of the Onsager reciprocal relations.

For applications, it is instructive to rewrite (14) in the form

$$\mathbf{E}_* = \hat{\mathcal{R}} \mathbf{j} - \hat{\alpha} \nabla T, \quad \mathbf{q} = -\hat{\alpha} T \mathbf{j} - \hat{\kappa} \nabla T, \quad (15)$$

where  $\hat{\mathcal{R}} = \hat{\sigma}^{-1}$ ,  $\hat{\kappa}$  and  $\hat{\alpha}$  are the tensors of electric resistivity, thermal conductivity and thermopower, respectively. Again, the same tensor  $\hat{\alpha}$  enters the expressions for  $\mathbf{E}_*$  and  $\mathbf{q}$  owing to the Onsager relations. The thermal conductivity and thermopower are given by  $\hat{\kappa} = \hat{\eta} - T \hat{\beta} \hat{\mathcal{R}} \hat{\beta}$  and  $\hat{\alpha} = \hat{\mathcal{R}} \hat{\beta}$ , respectively.

So far our consideration has been quite general, valid for the electron gas of any relativity and degeneracy. The analysis is considerably simplified for strongly degenerate electrons. In this case the main contribution to electron transport comes from the electrons with energies  $|\epsilon - \mu| \lesssim k_B T$  in the narrow thermal width of the Fermi level. Standard calculations yield

$$\hat{\sigma} = \frac{e^2 n_e \hat{A}}{m_* \Delta}, \quad \hat{\kappa} \approx \hat{\eta} = \frac{\pi^2 n_e k_B^2 T \hat{A}}{3 m_* \Delta}, \quad (16)$$

where  $\hat{A}$  is given by (12),  $\Delta$  is defined in (11),  $m_* = \mu/c^2$  is the effective electron mass at the Fermi surface ( $\mu$  includes  $m_e c^2$ ), while  $\omega$ ,  $\nu_a$  and  $\nu_p$  have to be taken at  $\epsilon = \mu$ . Note that  $\hat{\sigma}$  and  $\hat{\kappa}$  satisfy the Wiedemann-Franz law,

$$\hat{\kappa} = \frac{\pi^2 k_B^2 T}{3e^2} \hat{\sigma}, \quad (17)$$

which is natural for strongly degenerate electrons in the relaxation-time approximation (e.g. Ziman 1960).

The tensors  $\hat{\sigma}$  and  $\hat{\kappa}$  have similar structure, determined by the matrix  $\hat{A}$ . Therefore, either electric or thermal conduction is defined by six different transport coefficients of three types:

(i) Three diagonal terms ( $A_{xx}$ ,  $A_{yy}$ ,  $A_{zz}$ ) are generally different reflecting anisotropy of the transport along all three axes;

(ii) There are two basically different Hall coefficients ( $A_{xy} = -A_{yx}$ ;  $A_{yz} = -A_{zy}$ ) and two different Hall parameters,

$$x_a = \omega/\nu_a, \quad x_p = \omega/\nu_p, \quad (18)$$

associated with two collision frequencies,  $\nu_a$  and  $\nu_p$ ; they describe gyrotropic character of electron transport in a magnetic field;

## 4 D. G. Yakovlev

(iii) There are two equal coefficients  $A_{xz} = A_{zx}$  for non-vanishing  $B_x$  and  $B_z$ ;

(iv) One has  $A_{\alpha\beta}(\mathbf{B}) = A_{\beta\alpha}(-\mathbf{B})$ , in agreement with Onsager relations.

Naturally, the electron transport in nuclear pasta is richer in physics than in ordinary neutron star matter.

Let us present also the resistivity tensor

$$\hat{\mathcal{R}} = \frac{m_*}{e^2 n_e} \begin{pmatrix} \nu_p & \omega b_z & 0 \\ -\omega b_z & \nu_p & \omega b_x \\ 0 & -\omega b_x & \nu_a \end{pmatrix}. \quad (19)$$

Its structure is simpler than that of  $\hat{\sigma}$  or  $\hat{\kappa}$ .

If  $\hat{\sigma}$  is found from equation (16), one can calculate the thermopower tensor as

$$\hat{\alpha} = \frac{\pi^2 k_B^2 T \hat{\mathcal{R}}}{3e} \frac{\partial \hat{\sigma}(\mu)}{\partial \mu}. \quad (20)$$

Such relations are standard (Ziman 1960) for scalar thermopower of strongly degenerate electrons in the relaxation time approximation. Evidently, they remain valid for tensor quantities. In order to use them one should express  $\omega$ ,  $\nu_a$ , and  $\nu_p$  in  $\hat{\sigma}$  as functions of  $\epsilon$  and set  $\epsilon = \mu$ . In addition, one should express  $n_e$  through  $\mu$  and differentiate over  $\mu$  afterwards.

The presented expressions are sufficient to estimate the electron transport properties in one domain of nuclear pasta. Below we analyze the transport coefficients in limiting cases. Since the structure of  $\hat{\sigma}$  and  $\hat{\kappa}$  is the same, we will mainly discuss  $\hat{\sigma}$  meaning that one can immediately find  $\hat{\kappa}$  using equation (17).

### 2.2 No magnetic field

In the limit of  $\mathbf{B} \rightarrow 0$  the transport coefficients are greatly simplified,

$$\hat{\sigma} = \frac{e^2 n_e}{m_*} \begin{pmatrix} \nu_p^{-1} & 0 & 0 \\ 0 & \nu_p^{-1} & 0 \\ 0 & 0 & \nu_a^{-1} \end{pmatrix}. \quad (21)$$

Here, the conductivity is characterized by the two different kinetic coefficients, along and across the symmetry axis,

$$\sigma_{a0} = \frac{e^2 n_e}{\nu_a m_*}, \quad \sigma_{p0} = \frac{e^2 n_e}{\nu_p m_*}. \quad (22)$$

In phases I and III of nuclear rods or rod-like bubbles one expects  $\nu_p \gg \nu_a$  (Table 1). Then the conductivity  $\sigma_{a0}$  along the symmetry axis is much larger than the leading conductivity  $\sigma_{p0}$  across this axis. If we view the leading transport as ‘normal,’ then the transport in the perpendicular direction is abnormally fast. In phase II of nuclear slabs one has  $\nu_a \gg \nu_p$ . The normal leading transport along the symmetry axis is much slower than across it ( $\sigma_{a0} \ll \sigma_{p0}$ ). Finally, in phase IV of spherical bubbles  $\nu_a = \nu_p$ , so that the transport is isotropic (‘normal’ in all directions, as in ordinary neutron star crust).

### 2.3 Finite magnetic field along or across symmetry axis

If  $\mathbf{B} \neq 0$ , transport properties are generally complicated. The simplest case takes place if  $\mathbf{B}$  is directed along the symmetry axis.

Then

$$\hat{\sigma} = \frac{e^2 n_e}{m_* \nu_p (1 + x_p^2)} \begin{pmatrix} 1 & -x_p & 0 \\ x_p & 1 & 0 \\ 0 & 0 & \nu_p (1 + x_p^2) / \nu_a \end{pmatrix}. \quad (23)$$

The conductivity in the symmetry plane is gyrotropic (governed by the magnetic field and the collision frequency  $\nu_p$ ), while the conductivity along the symmetry axis is unaffected by  $\mathbf{B}$  and determined by  $\nu_a$ .

If  $\mathbf{B}$  lies in the symmetry plane, along the  $x$  axis, then

$$\hat{\sigma} = \frac{e^2 n_e}{m_* \nu_p (\nu_a \nu_p + \omega^2)} \begin{pmatrix} \nu_a \nu_p + \omega^2 & 0 & 0 \\ 0 & \nu_a \nu_p & -\omega \nu_p \\ 0 & \omega \nu_p & \nu_p^2 \end{pmatrix}. \quad (24)$$

The conductivity along  $\mathbf{B}$  is again unaffected by the magnetic field (being naturally determined by  $\nu_p$ ), while the conductivity in the  $yz$  plane (across  $\mathbf{B}$ ) is gyrotropic and regulated by  $\nu_p$  and  $\nu_a$ .

If  $\nu_a = \nu_p = \nu_0$ , the conductivity is the same as in a basically isotropic medium immersed in a magnetic field; see Section 2.6.

### 2.4 Three regimes

If we increase  $B$  from  $B = 0$ , the Hall parameters  $x_p$  and  $x_a$  grow up and the electron transport is affected by the magnetic field. The regime of sufficiently small (smaller than 1) Hall parameters corresponds to weakly magnetized electrons, whereas the regime of high (higher than 1) Hall parameters to strongly magnetized electrons. Because  $x_p$  and  $x_a$  are not equal, there is also the regime of intermediate magnetization in which the electrons are already magnetized with respect to one Hall parameter but are still not magnetized with respect to the other one. These three magnetization regimes have different effects on various conductivity components at different inclinations  $\theta$  of  $\mathbf{B}$  to the symmetry axis.

As for the  $B$ -dependence of the conductivity, all conductivity components are divided into non-Hall ( $xx$ ,  $yy$ ,  $zz$ , and  $zx$  ones) and Hall ones ( $yx$  and  $zy$ ); we do not mention associated non-diagonal components like  $xz$  or  $xy$ ). The non-Hall components are even functions of  $\omega \propto B$  while the Hall components are odd functions. In the limit of weak electron magnetization the diagonal components stay nearly constant, while  $\sigma_{zx}$  increases as  $B^2$ . All non-vanishing Hall components increase proportionally to  $B$ .

In the limit of high electron magnetization ( $x_a \gg 1$ ,  $x_p \gg 1$ ) we obtain

$$\hat{\sigma} = \frac{e^2 n_e}{m_* (\nu_p \sin^2 \theta + \nu_a \cos^2 \theta)} \times \begin{pmatrix} \sin^2 \theta + (x_a x_p)^{-1} & -x_a^{-1} \cos \theta & \cos \theta \sin \theta \\ x_a^{-1} \cos \theta & (x_a x_p)^{-1} & -x_p^{-1} \sin \theta \\ \cos \theta \sin \theta & x_p^{-1} \sin \theta & \cos^2 \theta + x_p^{-2} \end{pmatrix}. \quad (25)$$

With increasing  $B$  in this regime the non-Hall components either stay constant (as  $\sigma_{xx}$ ,  $\sigma_{zz}$  and  $\sigma_{zx}$ ) or decrease proportionally to  $B^{-2}$ , whereas the Hall components decrease as  $B^{-1}$ . The decrease of the conductivity components at strong magnetization is evidently explained by frequent rotation of electrons around magnetic field lines, with many rotations between successive collisions.

### 2.5 Resistivity

The structure of the electric resistivity tensor  $\hat{\mathcal{R}}$ , equation (19), is simpler than of the conductivity. The diagonal components  $\mathcal{R}_{xx} =$



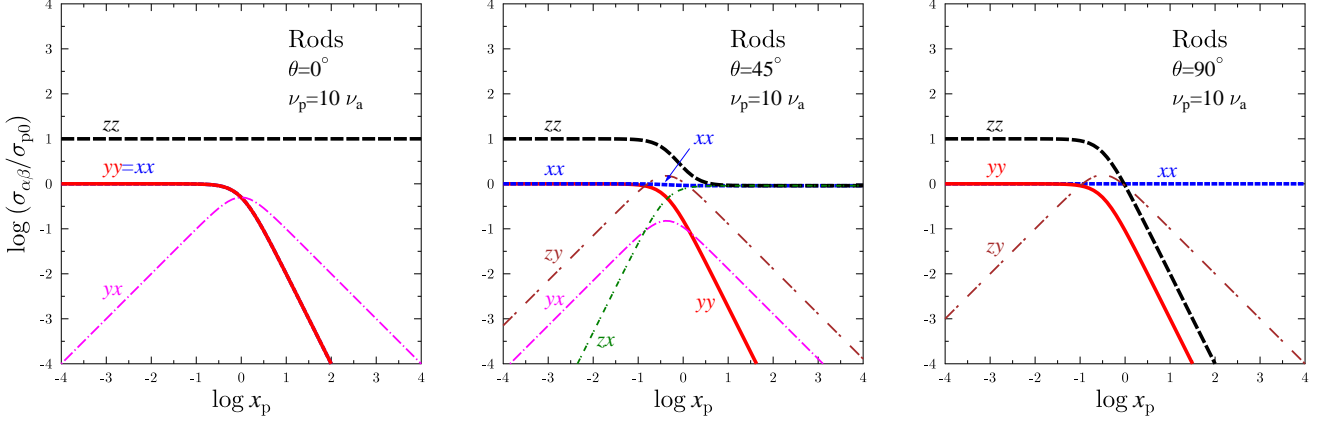


**Figure 1.** (Color online) Components of the electron conductivity tensor  $\sigma_{\alpha\beta}$  in phases I or III (in units of the leading conductivity  $\sigma_{p0}$  across the symmetry axis for  $\mathbf{B} = 0$ ) versus the leading Hall parameter  $x_b = \omega/\nu_b \propto B$  at three angles  $\theta = 0, 45$  and  $90^\circ$  (from left to right) between  $\mathbf{B}$  and the symmetry axis. The ratio of the effective electron collision frequencies across and along the symmetry axis is taken to be  $\nu_p/\nu_a = 10$ . Shown are all six generally different tensor components,  $\sigma_{xx}, \sigma_{yy}, \sigma_{zz}$  (thick lines of different types) and  $\sigma_{yx}, \sigma_{zx}$  and  $\sigma_{zy}$  (thin lines).

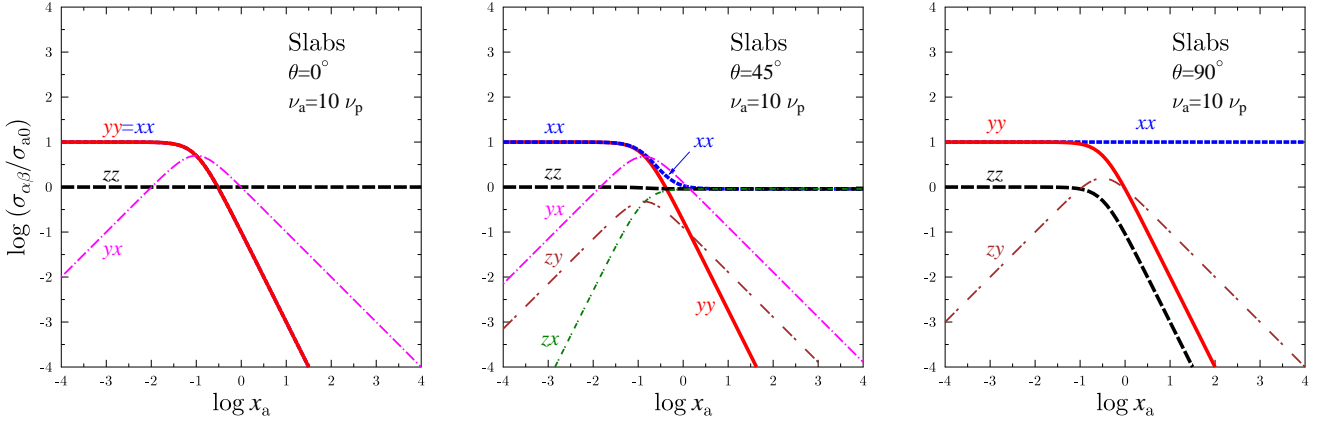


**Figure 2.** (Color online) Same as in Fig. 1 for electron conductivity tensor  $\sigma_{\alpha\beta}$  in phase II (in units of the leading conductivity  $\sigma_{a0}$  along the symmetry axis for  $\mathbf{B} = 0$ ) versus the leading Hall parameter  $x_a = \omega/\nu_a$  (proportional to  $B$ ) at  $\theta = 0, 45$  and  $90^\circ$  (from left to right) and  $\nu_a/\nu_p = 10$ .

$\mathcal{R}_{yy} \equiv \mathcal{R}_p$  and  $\mathcal{R}_{zz} = \mathcal{R}_a$  are totally independent of  $\mathbf{B}$ , being equal to corresponding inverse diagonal components (22) of the electric conductivity tensor at  $B = 0$ ,  $\mathcal{R}_p = 1/\sigma_{p0}$  and  $\mathcal{R}_a = 1/\sigma_{a0}$ . The leading resistivity ( $\mathcal{R}_p$  or  $\mathcal{R}_a$ ) is higher than the resistivity in the opposite direction. The Hall components  $\mathcal{R}_{xy} = -\mathcal{R}_{yx}$  and  $\mathcal{R}_{yz} = -\mathcal{R}_{zy}$  are directly proportional to  $\omega \propto B$ . In the regime of weak magnetization the diagonal components are larger than the Hall ones while in the regime of strong magnetization the Hall components are larger. Actually, there is only one non-trivial Hall component of  $\hat{\mathcal{R}}$  instead of two formal Hall components  $\mathcal{R}_{xy}$  and  $\mathcal{R}_{yz}$  in (19). To prove this one can rotate coordinate axes in the  $xz$  plane in such a way for the  $z$ -axis to become parallel to  $\mathbf{B}$ . After this rotation the tensor would contain the only one Hall component  $\mathcal{R}_{xy} = -\mathcal{R}_{yx} = m_*\omega/(e^2 n_e)$  totally independent of electron collision frequencies  $\nu_p$  and  $\nu_a$  (proving that the Hall components do not produce any dissipation although produce an important effect of Hall drift of the magnetic field). Such a rotation trick does not work out for conductivity tensors – there are generally two non-trivial Hall components of the conductivity.

The simplicity of the electric resistivity tensor is also pronounced in the expression for the Joule heat  $Q = (\mathbf{j} \cdot \hat{\mathcal{R}} \cdot \mathbf{j})$

[erg s<sup>-1</sup> cm<sup>-3</sup>],

$$Q = \mathcal{R}_p j_p^2 + \mathcal{R}_a j_a^2, \quad (26)$$

where  $j_p$  and  $j_a$  are the components of the electron current  $\mathbf{j}$  across and along the symmetry axis, respectively.

## 2.6 Phase of spherical bubbles

This phase is the simplest one because the medium is basically isotropic,  $\nu_a = \nu_p = \nu_0$ . The conductivity and resistivity tensors are especially simple in the coordinate system with the  $z$ -axis parallel to  $\mathbf{B}$ . For instance, the electric conductivity and resistivity tensors take the well known form

$$\hat{\sigma} = \begin{pmatrix} \sigma_{\perp} & -\sigma_H & 0 \\ \sigma_H & \sigma_{\perp} & 0 \\ 0 & 0 & \sigma_{\parallel} \end{pmatrix}, \quad \hat{\mathcal{R}} = \begin{pmatrix} \mathcal{R}_{\perp} & \mathcal{R}_H & 0 \\ -\mathcal{R}_H & \mathcal{R}_{\perp} & 0 \\ 0 & 0 & \mathcal{R}_{\parallel} \end{pmatrix}, \quad (27)$$

where the subscripts  $\parallel$  and  $\perp$  refer to conductivities and resistivities parallel and perpendicular to  $\mathbf{B}$ , respectively, while the subscript H labels the Hall terms. The Hall terms in  $\hat{\sigma}$  and  $\hat{\mathcal{R}}$  have naturally

different signs. The expressions for these components are

$$\begin{pmatrix} \sigma_{\parallel} \\ \sigma_{\perp} \\ \sigma_{\text{H}} \end{pmatrix} = \sigma_0 \begin{pmatrix} 1 \\ 1/(1+x^2) \\ x/(1+x^2) \end{pmatrix}, \quad \begin{pmatrix} \mathcal{R}_{\parallel} \\ \mathcal{R}_{\perp} \\ \mathcal{R}_{\text{H}} \end{pmatrix} = \frac{1}{\sigma_0} \begin{pmatrix} 1 \\ 1 \\ x \end{pmatrix}, \quad (28)$$

with  $\sigma_0 = e^2 n_e / \nu_0 m_*$ ,  $x = \omega / \nu_0$  being the single Hall parameter in the given case. Therefore,  $\sigma_{\parallel} = \sigma_0 = 1/\mathcal{R}_{\parallel} = 1/\mathcal{R}_{\perp}$  are independent of  $\mathbf{B}$ , and  $\mathcal{R}_{\text{H}} \propto B$ . In the regime of weak magnetization, at  $x \ll 1$ , one has nearly constant  $\sigma_{\perp} \approx \sigma_{\parallel}$  but  $\sigma_{\text{H}} \propto B$ , while at  $x \gg 1$  one has  $\sigma_{\perp} \propto B^{-2}$  and  $\sigma_{\text{H}} \propto B^{-1}$ .

### 2.7 Illustrative examples

By way of illustration, in Fig. 1 we show the components of the electron conductivity tensor  $\sigma_{\alpha\beta}$ , given by equations (16) and (12), in phases of rods or rod-like bubbles versus the leading Hall parameter  $x_p$ , equation (18). The components are expressed in terms of the leading ('normal') conductivity  $\sigma_{p0}$  at  $B = 0$ , equation (22). Recall that the presented ratio  $\sigma_{\alpha\beta}/\sigma_{p0}$  is the same as  $\kappa_{\alpha\beta}/\kappa_{p0}$ . The three panels correspond to the three inclination angles  $\theta = 0, 45$  and  $90^\circ$  of  $\mathbf{B}$  to the symmetry axis. The ratio of the leading and weaker electron collision frequencies is taken to be  $\nu_p/\nu_a = 10$ . We present all six different tensor components,  $\sigma_{xx}$ ,  $\sigma_{yy}$  and  $\sigma_{zz}$  (short-dashed, solid, and long-dashed thick lines, respectively), as well as  $\sigma_{yx}$ ,  $\sigma_{zx}$  and  $\sigma_{zy}$  (dot-dashed, short dot-dash-spaced and long dot-dash-spaced thin lines, respectively).

The conductivities plotted in the left-hand ( $\theta = 0$ ) and right-hand ( $\theta = 90^\circ$ ) panels are described in Section 2.3 (equations (23) and (24), respectively). At  $\theta = 0$  the conductivity  $\sigma_{zz}$  is unaffected by the field, being determined by the weaker collision frequency  $\nu_a$ . At  $\theta = 90^\circ$  the conductivity  $\sigma_{xx}$  is not affected by  $\mathbf{B}$ , being determined by  $\nu_p$ . If  $x_p \rightarrow 0$ , we reproduce the field-free limit (Section 2.2), with the leading ('normal')  $\sigma_{xx}$  and  $\sigma_{yy}$  conductivities 10 times smaller than the 'abnormal' conductivity  $\sigma_{zz}$  (because  $\nu_p/\nu_a = 10$ , in our example).

In the limit of weak electron magnetization the diagonal components stay nearly constant, while  $\sigma_{zx}$  grows as  $B^2$  and all non-vanishing Hall components increase as  $B$ . In the limit of high electron magnetization the non-Hall components either stay constant (as  $\sigma_{xx}$ ,  $\sigma_{zz}$  and  $\sigma_{zx}$  at  $\theta = 45^\circ$  in Fig. 1) or decrease as  $B^{-2}$  (like  $\sigma_{yy}$  in the same case). In this regime the Hall components decrease as  $B^{-1}$ .

Fig. 2 plots the same conductivities as in Fig. 1 for  $\theta = 0, 45$  and  $90^\circ$  but in phase II of nuclear slabs. The conductivities are expressed in units of the leading ('normal') conductivity  $\sigma_{a0}$  at  $B = 0$ , equation (22); they are shown as functions of the leading Hall parameter  $x_a$ . The ratio of the leading to weaker electron collision frequency is again assumed to be  $\nu_a/\nu_p = 10$ . The main features of the conductivities are similar to those in Fig. 1 for the phase of rods. In the regime of weak magnetization for slabs we also have the abnormal conductivities ( $\sigma_{xx}$  and  $\sigma_{yy}$ ) much higher than the 'normal' conductivity ( $\sigma_{zz}$ ).

## 3 AVERAGING OVER DOMAINS

In Section 2 we have considered the electron transport in one domain of exotic nuclear structures. This transport is described by  $3 \times 3$  matrices of kinetic coefficients; the matrix elements behave differently and strongly depend on the magnetic field  $\mathbf{B}$  and anisotropic properties of nuclear structures. Macroscopic equations

of electron heat and charge transport contain the conductivity (resistivity) tensors averaged over an ensemble of domains. In principle, the averaging should take into account correlation properties of electron transport in different domains. However, the theory of nuclear pasta phases is still not very elaborated (Section 1), so that no reliable information has been obtained about predominant orientations and other statistical properties of the domains.

Therefore, it seems instructive to consider the simplest model of freely oriented domains. We take the conductivity tensors obtained in Section 2 and average them over free orientations of the domains. It is evident, that after such averaging we obtain the conductivity tensors for basically isotropic medium in a magnetic field. In a coordinate frame with the  $z$ -axis along  $\mathbf{B}$ , the conductivity or resistivity tensors should have the same form (27) as in the phase of spherical bubbles (Section 2.6). Any tensor is characterized by three components which describe transport along and across  $\mathbf{B}$  as well as the Hall transport, although these components are generally more complicated than (28). Therefore, it is sufficient to determine these three components.

To this aim, let us take, for instance, the electric conductivity tensor (16) and calculate  $\sigma_{\parallel} = (\mathbf{b} \cdot \hat{\sigma} \cdot \mathbf{b})$ ,  $\sigma_{\perp} = (\mathbf{e}_1 \cdot \hat{\sigma} \cdot \mathbf{e}_1)$  and  $\sigma_{\text{H}} = (\mathbf{e}_1 \cdot \hat{\sigma} \cdot \mathbf{e}_2)$ , for a given orientation of the symmetry axis. Here,  $\mathbf{e}_1$  and  $\mathbf{e}_2$  are two orthogonal unit vectors perpendicular to  $\mathbf{b}$ , with  $\mathbf{e}_2 = \mathbf{e}_1 \times \mathbf{b}$ . We obtain

$$\begin{pmatrix} \sigma_{\parallel} \\ \sigma_{\perp} \\ \sigma_{\text{H}} \end{pmatrix} = \frac{e^2 n_e}{m_* \Delta} \begin{pmatrix} \nu_a \nu_p b_x^2 + \nu_p^2 b_z^2 + \omega^2 \\ \nu_a \nu_p (e_{1x}^2 + e_{1y}^2) + \nu_p^2 e_{1z}^2 \\ \nu_a \omega b_z^2 + \nu_p \omega b_x^2 + e_{1z} e_{2z} (\nu_p^2 - \nu_p \nu_a) \end{pmatrix}. \quad (29)$$

Now the averaging over orientations of nuclear clusters, which we denote as  $\langle \dots \rangle$ , is equivalent to averaging over rotation of the  $(\mathbf{e}_1, \mathbf{e}_2)$  plane about the  $\mathbf{b}$  axis and to subsequent averaging over orientations of the  $\mathbf{b}$  axis. These averagings can be done analytically with the result that in any reference frame with the  $z$  axis parallel to  $\mathbf{B}$

$$\langle \hat{\sigma} \rangle = \begin{pmatrix} \langle \sigma_{\perp} \rangle & -\langle \sigma_{\text{H}} \rangle & 0 \\ \langle \sigma_{\text{H}} \rangle & \langle \sigma_{\perp} \rangle & 0 \\ 0 & 0 & \langle \sigma_{\parallel} \rangle \end{pmatrix}. \quad (30)$$

The averaged conductivity components are given by

$$\begin{pmatrix} \langle \sigma_{\parallel} \rangle \\ \langle \sigma_{\perp} \rangle \\ \langle \sigma_{\text{H}} \rangle \end{pmatrix} = \frac{e^2 n_e}{m_* \omega^2} \begin{pmatrix} (\omega^2 + \nu_p^2)(\omega^2 + \nu_p \nu_a) H - \nu_p \\ \frac{1}{2} (\nu_a \nu_p (\omega^2 - \nu_p^2) H + \nu_p) \\ \omega - \omega \nu_a \nu_p^2 H \end{pmatrix}, \quad (31)$$

where

$$H = \begin{cases} (rs)^{-1} \arctan(s/r) & \text{at } \nu_a > \nu_p, \\ (2rs)^{-1} \ln[(r+s)/(r-s)] & \text{at } \nu_a < \nu_p, \\ 1/(\nu_a^3 + \omega^2 \nu_a) & \text{at } \nu_a = \nu_p, \end{cases} \quad (32)$$

with  $r = \sqrt{\nu_p(\omega^2 + \nu_a \nu_p)}$  and  $s = \omega \sqrt{|\nu_p - \nu_a|}$ .

All three conductivities  $\langle \sigma_{\parallel} \rangle$ ,  $\langle \sigma_{\perp} \rangle$ , and  $\langle \sigma_{\text{H}} \rangle$  depend generally on  $B$  (or on  $\omega$ ) and on collision frequencies  $\nu_a$  and  $\nu_p$ . In the limit of weak electron magnetization we naturally have  $\langle \sigma_{\parallel} \rangle = \langle \sigma_{\perp} \rangle = \langle \sigma_0 \rangle$ , where

$$\langle \sigma_0 \rangle = \frac{e^2 n_e \langle \nu^{-1} \rangle}{m_*}, \quad \langle \nu^{-1} \rangle = \frac{2}{3\nu_p} + \frac{1}{3\nu_a}; \quad (33)$$

$\langle \sigma_0 \rangle$  being the field-free averaged conductivity, and  $\langle \nu^{-1} \rangle$  the averaged inverse collision frequency (averaged relaxation time) of electrons;  $\langle \sigma_0 \rangle$  is given by the familiar Drude formula. According to (29) and (31), in the same limit of weak electron magnetization the

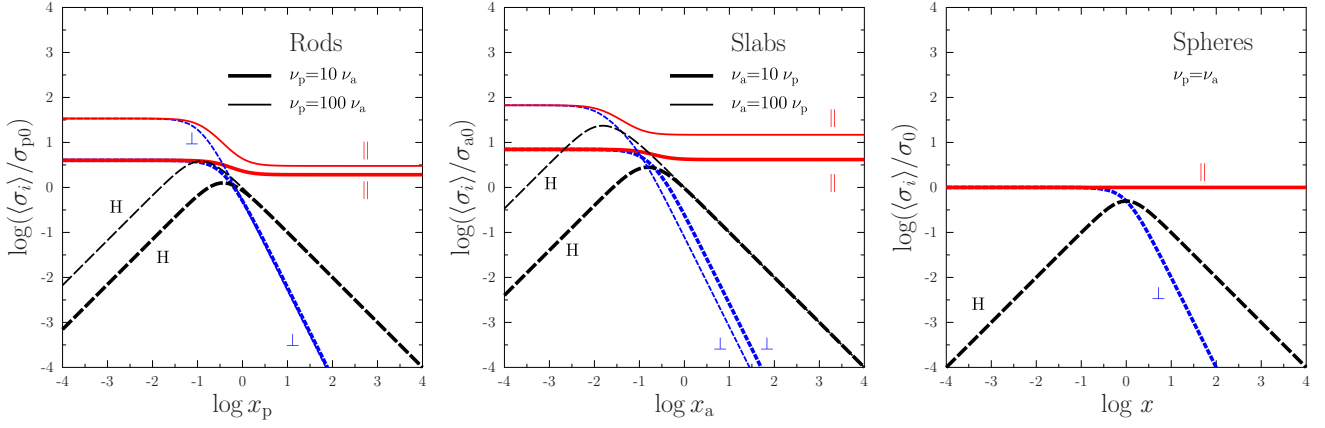


**Figure 3.** (Color online) Electron conductivities  $\langle\sigma_i\rangle$  (averaged over orientations of nuclear clusters, in units of the leading conductivities (22) at  $B = 0$ ) along  $\mathbf{B}$  ( $i = \parallel$ , solid lines), across  $\mathbf{B}$  ( $i = \perp$ , short-dashed lines), as well as the Hall conductivity ( $i = H$ , long-dashed lines) as functions of the leading Hall parameter for the phases of rods, slabs and spherical bubbles (from left to right). For rods and slabs the conductivities are given for two ratios of the leading to weaker collision frequencies, 10 and 100 (thick and thin lines, respectively). See text for details.

Hall term behaves as

$$\langle\sigma_H\rangle \approx \frac{e^2 n_e \langle\nu\rangle \omega}{m_* v_a^2 \nu_a} \propto B, \quad (34)$$

where  $\langle\nu\rangle = (\nu_a + 2\nu_p)/3$  is the angle averaged collision frequency.

For illustration, in Fig. 3 we show all three electron conductivities  $\langle\sigma_i\rangle$  averaged over orientations of domains, in units of the leading (‘normal’) conductivities at  $B = 0$ . The conductivities along  $\mathbf{B}$  ( $i = \parallel$ ) are plotted by solid lines, across  $\mathbf{B}$  ( $i = \perp$ ) by short-dashed lines, and the Hall conductivities ( $i = H$ ) by long-dashed lines. These conductivities are presented as functions of the leading Hall parameters (18) for the phases of rods, slabs and spherical bubbles (left, middle and right panels, respectively). For the phases of rods and slabs the conductivities are presented at two ratios of the leading to weaker collision frequencies, 10 and 100 (thick and thin lines, respectively).

As discussed above, in the weak magnetization regime the conductivities  $\langle\sigma_{\parallel}\rangle$  and  $\langle\sigma_{\perp}\rangle$  are almost equal and independent of  $\mathbf{B}$ . At large difference between  $\nu_a$  and  $\nu_p$  these conductivities are much larger than the corresponding ‘normal’ conductivities  $\sigma_{a0}$  or  $\sigma_{p0}$  (Section 2, equation (22)). This results from the presence of abnormally high conductivities in any domain. By averaging over orientations of domains we inevitably allow for abnormally high transport in any direction.

In the regime of strong magnetization the longitudinal conductivity, again, becomes independent of  $\mathbf{B}$ . However, it depends on  $\nu_a/\nu_p$  as

$$\langle\sigma_{\parallel}\rangle = \frac{e^2 n_e}{m_*} S, \quad (35)$$

where

$$S = \begin{cases} (\gamma\zeta)^{-1} \arctan(\zeta/\gamma) & \text{at } \nu_a > \nu_p, \\ (2\gamma\zeta)^{-1} \ln[(\gamma + \zeta)/(\gamma - \zeta)] & \text{at } \nu_a < \nu_p, \\ 1/\nu_a & \text{at } \nu_a = \nu_p, \end{cases} \quad (36)$$

with  $\gamma = \sqrt{\nu_p}$  and  $\zeta = \sqrt{|\nu_p - \nu_a|}$ . The higher the difference between  $\nu_a$  and  $\nu_p$ , the lower  $\langle\sigma_{\parallel}\rangle$  (measured in units of the leading field-free conductivity).

In phase of spheres  $\langle\sigma_{\parallel}\rangle$  is naturally independent of  $\mathbf{B}$  being equal to  $\langle\sigma_0\rangle$  at any  $\mathbf{B}$ .

As for the transverse averaged conductivity at high magnetization, it is suppressed with growing  $\mathbf{B}$  as  $\langle\sigma_{\perp}\rangle \propto B^{-2}$  (Fig. 3). The appropriate asymptote is

$$\langle\sigma_{\perp}\rangle = \frac{e^2 n_e \nu_p}{2m_* \omega^2} (1 + \nu_a S). \quad (37)$$

The averaged Hall conductivity at high magnetization behaves as  $\langle\sigma_H\rangle \propto B^{-1}$ . It is given by the universal asymptote

$$\langle\sigma_H\rangle \approx \frac{e^2 n_e}{m_* \omega}, \quad (38)$$

which is independent of collision frequencies (meaning that  $\langle\sigma_H\rangle$  becomes collisionless) and of specific pasta phase. In this regime,  $\langle\sigma_H\rangle$  is governed by classical Hall drift of electrons in crossed electric and magnetic fields (e.g., Pitaevskii & Lifshits 1981). Generally, the anisotropy of collision frequencies has larger effect on averaged conductivity components in phase of slabs than in phase of rods.

Finally, let us discuss the tensor of averaged resistivity  $\langle\hat{\mathcal{R}}\rangle$  which has the same form as (27). A simple averaging of the resistivity tensor (19) gives

$$\langle\mathcal{R}_{\parallel}\rangle = \langle\mathcal{R}_{\perp}\rangle = \langle\mathcal{R}_0\rangle = \frac{\langle\nu\rangle m_*}{e^2 n_e}, \quad \langle\mathcal{R}_H\rangle = \frac{\omega m_*}{e^2 n_e}. \quad (39)$$

This tensor has the same structure as the tensor (28) in phase of spheres. The only collision frequency involved here is the averaged collision frequency  $\langle\nu\rangle$ . It determines the averaged longitudinal and transverse resistivities which are equal and independent of  $\mathbf{B}$ . The Hall resistivity  $\langle\mathcal{R}_H\rangle$  exceeds  $\langle\mathcal{R}_0\rangle$  at high magnetization,  $\omega > \langle\nu\rangle$ .

Let us stress, that, generally,  $\langle\hat{\mathcal{R}}\rangle \neq \langle\hat{\sigma}\rangle^{-1}$  and the difference can be substantial in anisotropic media. While calculating Joule heat (26) one should definitely use the averaged resistivity, but not the inverse averaged conductivity. Large difference between  $\nu_a$  and  $\nu_p$  does not produce any significant difference between  $\langle\mathcal{R}_0\rangle$  and the leading non-averaged resistance ( $1/\sigma_{a0}$  or  $1/\sigma_{p0}$ ).

## 4 COLLISION FREQUENCIES

So far, we have treated the collision frequencies  $\nu_a$  and  $\nu_p$  as given. Let us discuss how to calculate them.

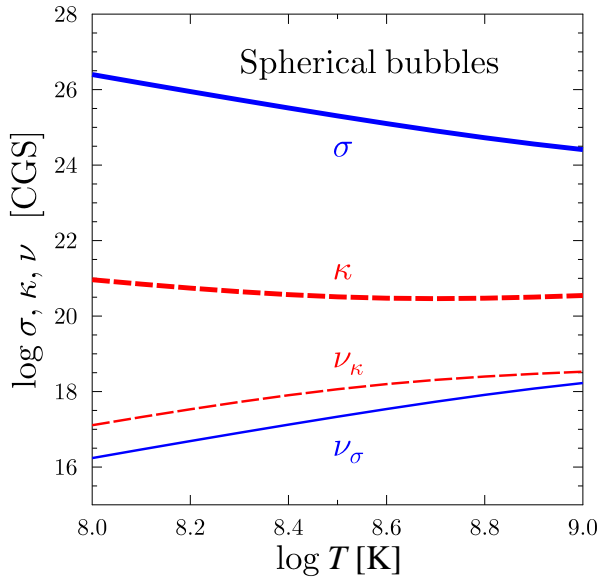


**Figure 4.** (Color online) Electric and thermal conductivities (thick solid and dashed lines, respectively) versus temperature in phase IV of spherical bubbles at  $\rho = 1.423 \times 10^{14} \text{ g cm}^{-3}$ . Thin solid and dashed lines show the effective collision frequencies  $\nu_\sigma$  and  $\nu_\kappa$  for electric and thermal conductivities, respectively. See text for details.

#### 4.1 Spherical bubbles

The formalism for calculating the collision frequency  $\nu_0$  ( $= \nu_a = \nu_p$ ) in phase IV of spherical bubbles is the same as that for spherical nuclei in the ordinary neutron star crust. For illustration, consider model I of Oyamatsu (1993), according to which spherical bubbles exist in the narrow density range (from about  $1.42 \times 10^{14}$  to  $1.43 \times 10^{14} \text{ g cm}^{-3}$ , Section 2.1), just near the interface between the mantle and neutron star core. Analytic fits for proton and neutron density profiles in nuclear bubbles are given by Haensel, Potekhin & Yakovlev (2007) in their Appendix B.

For certainty, we take  $\rho = 1.423 \times 10^{14} \text{ g cm}^{-3}$  (i.e., the baryon number density  $n_b = 0.08517 \text{ fm}^{-3}$ ) although the results are almost independent of density within such a narrow density range. The radius of a spherical Wigner-Seitz cell around one spherical bubble is  $R_{\text{WS}} = 15.4 \text{ fm}$ . The cell contains  $A_{\text{tot}} \approx 1300$  nucleons including  $Z_{\text{tot}} \approx 45$  protons. They are mainly free neutrons distributed almost uniformly. The neutron and proton density profiles within the cell decrease near the cell's center. This creates neutron and proton holes which can be collectively treated as a nuclear hole. The minimum neutron density in the center is only slightly lower than the average neutron density, while the central proton density drops to zero. The proton hole is equivalent to vacancies of  $Z_h \approx 11$  protons; whereas the entire nuclear hole is equivalent to vacancies of  $A_{\text{nuc}} \approx 48$  nucleons. The root-mean-squared radius of the proton hole is about 8.2 fm; the neutron hole is shallow but larger. These nuclear holes behave as charged quasiparticles and form a strongly coupled Coulomb system. The electrons are distributed almost uniformly and scatter off charge fluctuations of proton vacancies. The electron chemical potential is  $\mu \approx 87.3 \text{ MeV}$ . The electron transport properties can be calculated by applying standard formalism of electron transport in a plasma of spherical nuclei (Potekhin et al. 1999; Gnedin, Yakovlev & Potekhin 2001; Potekhin et al. 2013) and replacing the nuclei by the nuclear holes.

Fig. 4 shows the temperature dependence of the electric and

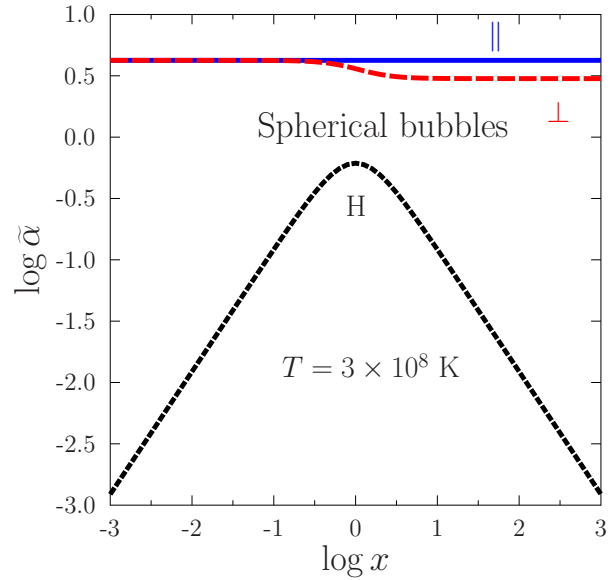


**Figure 5.** (Color online) Reduced dimensionless thermopower components  $\tilde{\alpha}_{\parallel}$ ,  $\tilde{\alpha}_{\perp}$  and  $\tilde{\alpha}_{\text{H}}$  (solid, long-dashed and short-dashed lines, respectively) given by (40) versus the Hall parameter  $x = \omega/\nu_\sigma$  in phase IV of spherical bubbles at  $\rho = 1.423 \times 10^{14} \text{ g cm}^{-3}$  and  $T = 3 \times 10^8 \text{ K}$ . See text for details.

thermal conductivities,  $\sigma$  and  $\kappa$  (thick lines), in the phase of spherical bubbles at  $\rho = 1.423 \times 10^{14} \text{ g cm}^{-3}$ . The conductivities are calculated with the method of quasi-potential for electron-nucleus scattering suggested by A. Y. Potekhin (Potekhin et al. 1999; Gnedin, Yakovlev & Potekhin 2001) and modified to consider electron scattering by nuclear holes. The calculations include Coulomb coupling of nuclear holes, Debye–Waller factor, multi-phonon processes, and shape of spherical bubbles. The results are more advanced than those based on the simplified model (7) of the collision integral in the relaxation time approximation. The displayed conductivities are solely produced by electron-hole scattering; other scattering mechanisms (e.g., the electron-electron scattering, Shternin & Yakovlev 2006) are disregarded. Low-temperature suppression of the electron-phonon scattering due to electron band structure effects (Chugunov 2012) is not included.

The conductivities  $\sigma$  and  $\kappa$  in Fig. 4 are expressed in CGS units (in  $\text{s}^{-1}$  and  $\text{erg cm}^{-1} \text{ s}^{-1} \text{ K}^{-1}$ , respectively). They are remarkably close to those calculated for standard models of inner neutron star crust of spherical nuclei (without nuclear pasta, e.g. Gnedin, Yakovlev & Potekhin 2001; Potekhin et al. 2013; note that the conductivities  $\sigma$  in fig. 7 of the latter paper are plotted – from top to bottom – for  $\log T=8, 8.5$  and 9, respectively). Two thin lines in Fig. 4 present the effective collision frequencies  $\nu_\sigma$  and  $\nu_\kappa$  (expressed in  $\text{s}^{-1}$ ) which describe the electric and thermal conduction, respectively (see, e.g., Potekhin et al. 1999). At  $T \gtrsim 10^9 \text{ K}$  these frequencies almost coincide. This means that the collision integral in the Boltzmann transport equation can be accurately described in the relaxation time approximation, equation (7). At lower temperatures  $\nu_\kappa$  becomes higher than  $\nu_\sigma$  and the relaxation time approximation is less accurate. However, at temperatures  $T \gtrsim 10^8 \text{ K}$ , most important for many applications, this approximation can still be used, at least for semi-quantitative analysis.

Having the effective collision frequency, we can easily estimate magnetic fields  $B = B_{\text{H}}$  which correspond to the Hall param-



eter  $x = \omega/\nu = 1$ . They are characteristic magnetic fields which affect the electron transport. For  $T = 10^8$  and  $10^9$  K with  $\nu = \nu_\sigma$  we obtain  $B_H \sim 2 \times 10^{11}$  and  $2 \times 10^{13}$  K, respectively. The  $B$  fields expected in neutron star interiors can be much higher. The lower the temperature, the lower the collision frequency, and the lower the fields which affect the electron transport.

So far we have not discussed the thermopower tensor  $\hat{\alpha}$ . For nuclear bubbles, we can present this tensor in the same form as  $\hat{\sigma}$ , equation (27), and write  $\hat{\alpha} = [\pi^2 k_B^2 T / (3e p_F \nu_F)] \hat{\tilde{\alpha}}$ , where  $\hat{\tilde{\alpha}}$  is the reduced (dimensionless) thermopower and  $\nu_F \approx c$  is the electron Fermi velocity. From equation (20) one obtains (Urpin & Yakovlev 1980)

$$\tilde{\alpha}_\parallel = 3 + \mathcal{P}, \quad \tilde{\alpha}_\perp = 3 + \frac{\mathcal{P}}{1 + x^2}, \quad \tilde{\alpha}_H = \frac{x\mathcal{P}}{1 + x^2}, \quad (40)$$

where  $\mathcal{P} = \partial \ln(\epsilon \nu_\sigma(\epsilon))^{-1} / \partial \ln p|_{p=p_F}$  and, again,  $x = \omega/\nu_\sigma = B/B_H$ . Note that the expression for  $\tilde{\alpha}_\parallel$  (which is independent of  $B$ ) is valid as long as the electrons are strongly degenerate, regardless of the applicability of the relaxation time approximation (7). In contrast, the expressions for  $\tilde{\alpha}_\perp$  and  $\tilde{\alpha}_H$  depend on  $B$  through  $x$  and require the approximation (7).

Fig. 5 presents all thermopower components for the phase of nuclear bubbles at  $\rho = 1.423 \times 10^{14}$  g cm<sup>-3</sup> and  $T = 3 \times 10^8$  K as a function of  $x = B/B_H$ , with  $B_H \approx 2.03 \times 10^{12}$  G. The thermopower  $\tilde{\alpha}_\parallel$  along the magnetic field is shown by the solid line, while  $\tilde{\alpha}_\perp$  and  $\tilde{\alpha}_H$  are plotted by the long-dashed and short-dashed lines, respectively. Recall that the thermopower components, contrary to the components of  $\hat{\sigma}$ ,  $\hat{\kappa}$  and  $\hat{\mathcal{R}}$ , can change sign depending on electron scattering mechanism. Signs of the thermopower components are regulated by the parameter  $\mathcal{P}$ . As shown by Urpin & Yakovlev (1980), neglecting the effects of the Debye-Waller factor and finite sizes of atomic nuclei, one has  $\mathcal{P} = -1$  for scattering of ultrarelativistic degenerate electrons in high-temperature crystals (when the relaxation time approximation is strictly valid). Indeed, we reproduce  $\mathcal{P} = -1$  at  $T = 10^9$  K when the relaxation time approximation is really accurate (see above). However, taking into account the Debye-Waller factor and finite sizes of the nuclei, we obtain  $\mathcal{P} \approx 1.1$  (instead of  $-1$ ). Therefore, at the bottom of the neutron star crust the effects of the Debye-Waller factor and of the shape of proton (proton hole) charge distribution are very important. If we decrease the temperature from  $10^9$  to  $10^8$  K, the relaxation time approximation becomes less accurate and  $\mathcal{P}$  increases slowly from 1.1 to 1.3.

According to Fig. 5, the magnetic field modifies  $\tilde{\alpha}_\perp$  but not very strongly. However, it significantly affects  $\tilde{\alpha}_H$  which regulates the Hall drift of the magnetic field. At  $x \lesssim 1$  the Hall thermopower directly determines the drift velocity (Urpin & Yakovlev 1980). Actually, the thermopower can be large enough to affect generation and evolution of magnetic fields in hot neutron stars.

## 4.2 Non-spherical nuclear structures

Calculations of  $\nu_a$  and  $\nu_p$  for phases I–III of non-spherical nuclear structures are much more complicated. In principle, they can be performed using the technique similar to that for spherical nuclei. To this aim one needs detailed studies of proton charge fluctuations and their effects on electron scattering. For instance, useful information on vibration properties of nuclear clusters can be obtained using their elastic constants (e.g., Pethick & Potekhin 1998). Proton charge fluctuations for the phase of slabs have been analyzed briefly by Watanabe, Iida & Sato (2000). Classical molecular dynamics simulations of dynamical behavior of nuclear pasta

have been conducted by Horowitz et al. (2005). However, these results seem insufficient for a reliable determination of  $\nu_a$  and  $\nu_p$ . The required physical ingredients are the effective structure factor  $S(\mathbf{q})$ , Debye-Waller factor and nuclear form-factor  $F(\mathbf{q})$ . Because nuclear clusters are non-spherical, these quantities will strongly depend on orientation of wave vector  $\mathbf{q}$ , leading to essential difference between  $\nu_a$  and  $\nu_p$ . To the best of our knowledge, the collision frequencies  $\nu_a$  and  $\nu_p$  for non-spherical clusters have not been calculated.

In this situation, it seems reasonable to assume that the leading effective frequency,  $\nu_a$  or  $\nu_p$ , is close to that for models of neutron star matter with spherical nuclei, while the other (abnormal) effective frequency is smaller. The ratio of the leading to the smaller frequency can be considered as a free parameter, ranging within reasonable limits, for instance, from 10 to 100. It would be difficult to be more exact using existing calculations. For illustration, one may look at fig 3 of Shternin & Yakovlev (2006) which shows partial thermal conductivities of electrons at  $B = 0$  in a neutron star crust of spherical nuclei. Assume the presence of nuclear pasta at the crust bottom and take the leading collision frequency the same as for electron–nucleus scattering in fig 3. Let the weaker collision frequency be limited by electron–electron collisions (whose contribution is also plotted in fig 3). Then in the temperature range  $10^8 - 10^9$  K the ratio of the leading to weaker collision frequencies would be  $\sim 10$ . Accurate microscopic calculations of  $\nu_a$  and  $\nu_p$  would be highly desirable.

## 5 CONCLUSIONS

We have analyzed electron transport in possible nuclear pasta phases in a mantle of magnetized neutron star. Specifically, we have performed model calculations of the tensors of electric and thermal conductivity,  $\hat{\sigma}$  and  $\hat{\kappa}$ , thermopower,  $\hat{\alpha}$ , and electric resistivity  $\hat{\mathcal{R}}$ . The model assumes the presence of domains containing (quasi)-ordered exotic nuclear structures of one type (rods, slabs, rod-like bubbles, or spherical bubbles; Table 1). The collision integral in the electron transport equation is described in the generalized relaxation time approximation (8) with two, generally different, effective collision frequencies,  $\nu_a$  and  $\nu_p$ , along and across the symmetry axis of corresponding nuclear clusters. For non-spherical nuclear clusters one can expect the presence of the leading (normal) collision frequency ( $\nu_a$  or  $\nu_p$ ) and abnormally weak frequency (Table 1), whereas for spherical bubbles  $\nu_a = \nu_p$ . Our model is simple but it allows us to include the effects of strong magnetic fields which would be difficult to do using more complicated models.

In Section 2 we have studied the electron transport in one domain and have found it rather complicated, with six generally different components of conductivity tensors.

In Section 3 we have considered electron transport in matter containing freely oriented domains of one type. The tensors of kinetic coefficients (30), (31), and (39) averaged over orientations of the domains are calculated analytically and have much simpler structure than their non-averaged counterparts. Each tensor contains only three different components, along and across  $\mathbf{B}$ , as well as the Hall component. These components show sufficiently simple dependence on  $\mathbf{B}$ . Nevertheless, this dependence is less trivial than in ordinary basically isotropic media with  $\nu_a = \nu_p$ . For instance the angle-averaged longitudinal conductivities  $\langle \sigma_\parallel \rangle$  and  $\langle \kappa_\parallel \rangle$  depend now on  $B$  and can be much higher than the leading normal conductivities (22) for  $B = 0$  determined by the leading collision frequencies. This enhancement of averaged longitudinal conduc-

tion is produced by the contribution of abnormally high conduction with lower collision frequency. The enhancement contradicts some expectations (e.g., Pons, Viganò & Rea 2013; Horowitz et al. 2015) that nuclear pasta suppresses the conduction. It seems both possibilities (suppression and enhancement) can be realized; see below.

In Section 4 we have outlined how to calculate the collision frequencies  $\nu_a$  and  $\nu_p$ . The collision frequencies and transport properties in phase of nuclear bubbles can be calculated rather reliably; they appear similar to those in traditional phase of spherical nuclei. However, the collision frequencies for non-spherical nuclear clusters are uncertain and require further attention.

Much work should be done to clarify transport properties of nuclear pasta. The major problem is to reliably calculate effective collision frequencies  $\nu_a$  and  $\nu_p$  for non-spherical nuclear clusters I–III (as outlined in Section 4.2). The problem requires accurate studies of proton charge fluctuations in these structures.

We have treated nuclear clusters in one domain as ordered and having the same shapes. If the ordering is not exact and the parameters (e.g.,  $\nu_a$  and  $\nu_p$ ) strongly vary, an additional averaging over disorder and parameter distributions has to be performed. We have assumed that orientations of domains are free. If not, more complicated averaging over orientations is needed.

We have neglected quantum oscillations of electron kinetic coefficients in very strong magnetic fields due to population of new electron Landau levels with increasing density (e.g., Potekhin 1999). If the electrons occupy many Landau levels, these oscillations are not too strong and our results should reproduce oscillation-averaged kinetic properties. In addition, since nuclear clusters are loosely bound, very strong magnetic fields may influence proton charge fluctuations and affect transport properties in this way. All these problems are beyond the scope of this paper.

Another, more serious problem would be to account for possible impurities and defects in nuclear pasta. It seems that these effects can greatly enhance or suppress electron transport.

Finally, let us stress, that there are other heat and charge transport mechanisms in nuclear pasta which should be taken into account along with the mechanisms studied above. For instance, one should bear in mind thermal conductivity due to electron-electron collisions (e.g. Shternin & Yakovlev 2006) and due to superfluid phonons (Aguilera et al. 2009) associated with the presence of free superfluid neutrons.

The results of the present studies can be useful for modeling of thermal relaxation between crust and core in young neutron stars and also in accreting neutron stars in X-ray transients with the crust overheated during accretion episodes (e.g., Pons, Viganò & Rea 2013). In addition, the results can be used to study evolution of magnetic fields in neutron stars and related phenomena (e.g., Horowitz et al. 2015).

## ACKNOWLEDGMENTS

This work was supported by the Russian Science Foundation, grant 14-12-00316.

## REFERENCES

Aguilera D. N., Cirigliano V., Pons J. A., Reddy S., Sharma R., 2009, *Physical Review Letters*, 102, 091101  
 Alcain P. N., Giménez Molinelli P. A., Dorso C. O., 2014, *Phys. Rev. C*, 90, 065803

Askerov B. M., 1981, *Electron Transport Phenomena in Semiconductors*. World Scientific, Singapore  
 Caplan M. E., Schneider A. S., Horowitz C. J., Berry D. K., 2015, *Phys. Rev. C*, 91, 065802  
 Chugunov A. I., 2012, *Astronomy Letters*, 38, 25  
 Dorso C. O., Giménez Molinelli P. A., López J. A., 2012, *Phys. Rev. C*, 86, 055805  
 Gnedin O. Y., Yakovlev D. G., Potekhin A. Y., 2001, *MNRAS*, 324, 725  
 Grill F., Pais H., Providência C., Vidaña I., Avancini S. S., 2014, *Phys. Rev. C*, 90, 045803  
 Gusakov M. E., Yakovlev D. G., Haensel P., Gnedin O. Y., 2004, *A&A*, 421, 1143  
 Haensel P., Potekhin A. Y., Yakovlev D. G., 2007, *Astrophysics and Space Science Library*, Vol. 326, *Neutron Stars. 1. Equation of State and Structure*. Springer, New York  
 Hashimoto M., Seki H., Yamada M., 1984, *Prog. Theor. Phys.*, 71, 320  
 Horowitz C. J., Berry D. K., Briggs C. M., Caplan M. E., Cumming A., Schneider A. S., 2015, *Physical Review Letters*, 114, 031102  
 Horowitz C. J., Pérez-García M. A., Berry D. K., Piekarewicz J., 2005, *Phys. Rev. C*, 72, 035801  
 Horowitz C. J., Pérez-García M. A., Carriere J., Berry D. K., Piekarewicz J., 2004, *Phys. Rev. C*, 70, 065806  
 Kaminker A. D., Pethick C. J., Potekhin A. Y., Thorsson V., Yakovlev D. G., 1999, *A&A*, 343, 1009  
 Kido T., Maruyama T., Niita K., Chiba S., 2000, *Nucl. Phys. A*, 663, 877  
 Lorenz C. P., Ravenhall D. G., Pethick C. J., 1993, *Physical Review Letters*, 70, 379  
 Maruyama T., Niita K., Oyamatsu K., Maruyama T., Chiba S., Iwamoto A., 1998, *Phys. Rev. C*, 57, 655  
 Nakazato K., Oyamatsu K., Yamada S., 2009, *Physical Review Letters*, 103, 132501  
 Okamoto M., Maruyama T., Yabana K., Tatsumi T., 2013, *Phys. Rev. C*, 88, 025801  
 Oyamatsu K., 1993, *Nucl. Phys. A*, 561, 431  
 Pethick C. J., Potekhin A. Y., 1998, *Phys. Lett. B*, 427, 7  
 Pitaevskii L. P., Lifshits E. M., 1981, *Physical Kinetics*. Butterworth-Heinemann, Oxford  
 Pons J. A., Viganò D., Rea N., 2013, *Nature Physics*, 9, 431  
 Potekhin A. Y., 1999, *A&A*, 351, 787  
 Potekhin A. Y., Baiko D. A., Haensel P., Yakovlev D. G., 1999, *A&A*, 346, 345  
 Potekhin A. Y., Fantina A. F., Chamel N., Pearson J. M., Goriely S., 2013, *A&A*, 560, A48  
 Ravenhall D. G., Pethick C. J., Wilson J. R., 1983, *Physical Review Letters*, 50, 2066  
 Schneider A. S., Berry D. K., Briggs C. M., Caplan M. E., Horowitz C. J., 2014, *Phys. Rev. C*, 90, 055805  
 Schuettrumpf B., Klatt M. A., Iida K., Schröder-Turk G. E., Maruhn J. A., Mecke K., Reinhard P.-G., 2015, *Phys. Rev. C*, 91, 025801  
 Shapiro S. L., Teukolsky S. A., 1983, *Black Holes, White Dwarfs, and Neutron Stars: The physics of compact objects*. Wiley-Interscience, New York  
 Shternin P. S., Yakovlev D. G., 2006, *Phys. Rev. D*, 74, 043004  
 Urpin V. A., Yakovlev D. G., 1980, *Sov. Astron.*, 24, 425  
 Watanabe G., Iida K., 2003, *Phys. Rev. C*, 68, 045801  
 Watanabe G., Iida K., Sato K., 2000, *Nucl. Phys. A*, 676, 455

Watanabe G., Sato K., Yasuoka K., Ebisuzaki T., 2002, Phys. Rev. C, 66, 012801

Williams R. D., Koonin S. E., 1985, Nucl. Phys. A, 435, 844

Ziman J. M., 1960, Electrons and Phonons. Clarendon Press, Oxford